Article

Influence of Carbon Cap on Self-Diffusion in Silicon Carbide

Marianne Etzelmüller Bathen [1,*], Margareta Linnarsson [2], Misagh Ghezellou [3], Jawad Ul Hassan [3] and Lasse Vines [1]

1. Department of Physics, Centre for Materials Science and Nanotechnology, University of Oslo, N-0316 Oslo, Norway; lasse.vines@fys.uio.no
2. Materials and Nanophysics, Department of Applied Physics, SCI, KTH Royal Institute of Technology, SE-106 91 Stockholm, Sweden; marga@kth.se
3. Department of Physics, Chemistry and Biology, Linköping University, SE-58183 Linköping, Sweden; misagh.ghezellou@liu.se (M.G.); jawad.ul-hassan@liu.se (J.U.H.)

* Correspondence: m.e.bathen@fys.uio.no

Received: 23 June 2020; Accepted: 24 August 2020; Published: 26 August 2020

Abstract: Self-diffusion of carbon (^{12}C and ^{13}C) and silicon (^{28}Si and ^{30}Si) in 4H silicon carbide has been investigated by utilizing a structure containing an isotope purified 4H-^{28}Si^{12}C epitaxial layer grown on an n-type (0001) 4H-SiC substrate, and finally covered by a carbon capping layer (C-cap). The ^{13}C and ^{30}Si isotope profiles were monitored using secondary ion mass spectrometry (SIMS) following successive heat treatments performed at 2300–2450 °C in Ar atmosphere using an inductively heated furnace. The ^{30}Si profiles show little redistribution within the studied temperature range, with the extracted diffusion lengths for Si being within the error bar for surface roughening during annealing, as determined by profilometer measurements. On the other hand, a significant diffusion of ^{13}C was observed into the isotope purified layer from both the substrate and the C-cap. A diffusivity of $D = 8.3 \times 10^6 e^{-10.4/k_B T}$ cm^2/s for ^{13}C was extracted, in contrast to previous findings that yielded lower both pre-factors and activation energies for C self-diffusion in SiC. The discrepancy between the present measurements and previous theoretical and experimental works is ascribed to the presence of the C-cap, which is responsible for continuous injection of C interstitials during annealing, and thereby suppressing the vacancy mediated diffusion.

Keywords: self-diffusion; silicon carbide; Carbon cap

---

1. Introduction

Self-diffusion of atomic species is a fundamental process in semiconductors, and vital for understanding both the thermally induced melting process and diffusion of impurities which are introduced during growth and doping. In silicon carbide, self-diffusion has been investigated extensively using both experimental [1–6] and theoretical [7,8] methods, but with conflicting results. Initially, carbon self-diffusion was predicted to have an energy barrier of $E_A = 7.4$ eV in intrinsic 6H-SiC [2] using ^{14}C radio-tracer techniques, with silicon diffusivities being more than 2 orders of magnitude lower than those for carbon [2,3]. Later, secondary ion mass spectrometry (SIMS) experiments on the 4H polytype yielded activation energies for ^{13}C self-diffusion of 8.5 eV [5] and 7.6 eV [6]. Interestingly, the findings of Ref. [6] suggested that Si and C diffusivities are of comparable magnitudes, in contrast to that of Hong et al. [2] and Hon et al. [3]. Although the experiments provide hints as to the mediating species for C and Si self-diffusion in SiC, they are not conclusive, with Ref. [5] predicting vacancy-mediated C self-diffusion and Ref. [6] proposing an interstitial-mediated mechanism, both on the C sub-lattice. Moreover, reported diffusivity values

for Si differ by several orders of magnitude. Note, however, that for high temperature annealing of SiC material and devices, a carbon cap is typically utilized in order to suppress the loss of surface atoms (in particular Si) and prevent surface roughening [9–11]. This may influence the migration mechanisms, further complicating the interpretation and understanding of self-diffusion in SiC.

The main intrinsic defects relevant for self-diffusion processes in SiC are the Si and C vacancies (V_{Si} and V_C), interstitials (Si_i and C_i), and antisites (Si_C and C_{Si}). The antisite defects have proven challenging to detect experimentally in 4H-SiC, potentially due to their predicted lack of charge state transition levels in the upper portion of the band-gap [12]. The vacancies and interstitials, on the other hand, are all electrically active in 4H-SiC, and behave as deep electron or hole traps in n-type or p-type material, respectively [12–14]. Hence, their presence is strongly detrimental to power electronics applications, and V_C is in fact known to be a prominent minority lifetime killer in 4H-SiC [15]. Conversely, V_{Si} is a high-spin single-photon emitter, showing considerable promise for quantum technology applications [16].

Density functional theory (DFT) has been used to investigate the mechanism for Si and C self-diffusion in SiC. When assessing the predicted activation energy for self-diffusion using DFT, we proceed by considering each defect species individually. First, a Fermi level range relevant for the annealing temperature being used is chosen, then the relevant defect charge state is identified, and finally the corresponding formation energy and energy barrier for migration are combined to form the activation energy for self-diffusion. This was done for several candidate defects in SiC in, e.g., Ref. [7]. Note that defect migration is anisotropic in 4H-SiC, often with higher barriers for migration between than within lattice planes. For the mid-gap Fermi levels (E_F) which manifest during the high-temperature heat treatments needed to induce migration in n-type 4H-SiC, V_C is expected to occupy the neutral or positive charge state [12,13], while V_{Si} will be negatively charged [14]. Both antisites are likely neutral, which is the case for the carbon interstitial as well, while Si_i defects reside in either the $q = 2+$ or $q = 4+$ charge state depending on whether they occupy a hexagonal (h) or pseudo-cubic (k) lattice plane in 4H-SiC, respectively [12].

Carbon vacancy migration was studied in-depth and for different migration paths using density functional theory in Ref. [17] in combination with the Heyd–Scuseria–Ernzerhof (HSE06) screened hybrid functional [18], the nudged elastic band [19,20] and dimer [21] methods, and comparing to experimental data, resulting in energy barriers for V_C^0 migration of 3.7–4.2 eV. In Ref. [22] Monte Carlo methods were instead employed, yielding migration barriers of 4.2–4.4 eV for the neutral charge state, while studies using the Perdew–Burke–Ernzerhof (PBE) functional [23] yield lower values of 3.3–3.5 eV for the same charge state of V_C [7,24]. Using the PBE functional is known to produce lower energies than, e.g., HSE06 as a result of underestimating the SiC band gap, which likely explains the lower values found in Refs. [7,24] as compared to Refs. [17,22]. Moreover, the calculations of Ref. [24] were not able to capture the full energetics of V_C, as no negative-U characteristics were shown for the $V_C(0/2-)$ transition [25], and Ref. [7] focused on the 3C polytype only. The HSE06-level values of Ref. [17] are therefore quoted for V_C^0 migration herein, using the axial barriers for V_C diffusion along the c-direction.

Migration of V_{Si} is an emerging popular focus [22,24,26] due to the qubit potential of the Si vacancy [16]. Under intrinsic conditions, V_{Si} inhabits the negative charge state, with predicted inter-planar migration barriers of 3.2–4.2 eV [22,24,26]. Interstitial defects are somewhat less studied than vacancies in 4H-SiC, perhaps on account of their greater complexity compared to the vacancies with more fixed lattice positioning. Migration barriers (E_A for migration) for both Si and C interstitials were estimated at ~ 1 eV in Ref. [27], but lattice configuration and Fermi level dependence were not discussed. Refs. [7,24] incorporated the charge state dependence of E_A for migration of Si_i and C_i, yielding barriers between 0.1–2 eV for both defect species and different migration paths. Using PBE and combining the formation and migration energies, Ref. [7] estimated activation energies for C self-diffusion in 3C-SiC (for $q = 0$) at around 7 eV via both C vacancies and interstitials, while that for Si was accompanied by higher barriers in the 8–12 eV range. An even more complete picture was

painted in Ref. [8], where self-diffusion of C and Si via their respective self-interstitials was studied while incorporating both temperature and entropy effects, although for 3C-SiC only. Here, activation energies for self-diffusion of carbon via C_i in 3C-SiC were estimated at 7.1 eV and 7.8 eV under C rich conditions for the neutral and doubly positive charge state, respectively. Si self-diffusion via Si_i was accompanied by much higher barriers, in the 10–11 eV range [8].

The available defect species for mediating self-diffusion in 4H-SiC, their charge state(s) when E_F resides at mid-gap, and the corresponding formation energy and migration barrier as collected from the literature are summarized in Table 1. C self-diffusion via C interstitials and vacancies appears to be separated by an energy difference of up to 1.5 eV, while E_A for Si self-diffusion is predicted in the 10–11 eV range regardless of whether Si_i or V_{Si} is responsible for mediation. Notice also that antisite defects are accompanied by large activation energies for self-diffusion around 13–15 eV, which translates into the interstitial and vacancy defects being more likely candidates for mediating thermally induced Si and C redistribution from their lattice sites in SiC.

Table 1. Calculated activation energies (E_A) for self-diffusion collected from the literature, defined as the sum of the formation energy and energy barrier for migration, via the various defect species available in 4H-SiC. During high-temperature annealing, the Fermi level (E_F) is located near mid-gap in the 4H-SiC samples, and the formation energy is quoted for this value of E_F. All formation energies are, wherever possible, quoted for Si poor and C rich conditions. Formation energies are quoted for HSE06 calculations, while the migration barriers are mostly deduced at PBE-level.

Defect Type	q When E_F = Mid-Gap	Formation Energy (eV)	Migration Barrier (eV)	E_A For Self-Diffusion
V_C	+ or 0	4.8 eV [13,17]	4.2 eV [17]	9.0 eV, 7.9 eV [7] (3C)
C_i	0	6.3 eV [12], 6.5 eV [24]	∼1 eV [27], 0.9 eV [24]	7.5 eV, 7.1 eV [8] (3C), 6.6 eV [7] (3C)
C_{Si}	0	3 eV [24]	∼10 eV [24]	13 eV
V_{Si}	−	7.0 eV [14]	4.2 eV [26], 3 eV [22]	10–11 eV
$Si_i(h)$	2+	8.5 eV [12]	∼1 eV [27]	∼9.5 eV, 10.2 eV (3C) [8]
$Si_i(k)$	4+	9.5 eV [12]	∼1 eV [27], 1.8 eV [24]	∼10.5 eV, ∼11 eV (3C) [8]
Si_C	0	5 eV [24]	∼10 eV [24]	15 eV

In the present work, we revisit the concept of self-diffusion in the 4H SiC polytype. By studying the motion of both C and Si within the same sample, we attempt to establish whether Si self-diffusion enthalpies are comparable to those of C or not, as the literature is not conclusive in this regard. An important feature of the present study is the use of a carbon cap (C-cap) covering the 4H-SiC surface during annealing to reduce the loss of Si from the surface and thereby suppressing surface roughening. However, the C-cap also presents a continuous injection channel for C interstitials from the C-cap/4H-SiC interface towards the 4H-SiC bulk. By comparing the present and previous experiments, we find that the mechanism for self-diffusion is significantly affected by the presence of the C-cap. In fact, the pre-factors for diffusion are several orders of magnitude higher when the C-cap is present as compared to the cap-free case, indicating a mechanism involving Frenkel pair formation in the sample bulk for self-diffusion.

2. Methods

An epitaxial layer (epi-layer) of 4H-$^{28}Si^{12}C$ silicon carbide was grown by chemical vapor deposition (CVD) on a n-type (0001) 4H-SiC substrate at the University of Linköping. The CVD-grown layer is ∼7 µm thick, and the isotope purity is estimated to be $^{28}Si > 99.85\%$ and $^{12}C > 99.98\%$. A C-cap was applied to all samples prior to annealing by graphitizing a photoresist film at 900 °C on the sample surface, in order to avoid surface roughening during the elevated heat treatments. The samples were subjected to high temperature treatments employing an inductively heated furnace (RFA) holding Ar atmosphere in the temperature range 2300–2450 °C. A Cameca IMS7f Secondary Ion Mass Spectrometer (SIMS) equipped with an O_2 primary ion beam source was used to measure the concentration versus depth profiles of Si and C. Absolute concentration values were obtained by

assuming natural abundance in the substrate. For depth calibration, the sputtered crater depths were measured by a Dektak 8 stylus profilometer and a constant erosion rate was assumed.

The diffusion profiles were fitted according to the error function

$$c = c_2 + \frac{c_1 - c_2}{2}\mathrm{erfc}\left\{\frac{x-d}{2\sqrt{Dt}}\right\} \tag{1}$$

to extract the ^{13}C diffusivities (D) at each temperature, where c is the concentration, t the annealing time, x denotes the depth and d the interface position. Moreover, c_1 and c_2 define the boundary conditions at $t = 0$ for $x - d \leq 0$ and $x - d > 0$, respectively. Finally, the diffusion parameters for the migrating species were determined according to an Arrhenius model

$$D = D_0 e^{-E_\mathrm{A}/k_\mathrm{B}T}, \tag{2}$$

with D_0 being the exponential pre-factor for diffusion, E_A the activation energy for self-diffusion, k_B the Boltzmann constant, and T the annealing temperature.

Surface roughness will broaden the measured SIMS profiles. To account for this extra broadening, the surface irregularities have been included as root mean square (rms) values and the measured diffusion coefficients have been corrected according to

$$\sigma_D = \sqrt{\sigma_M^2 - \mathrm{rms}^2}, \tag{3}$$

where $\sigma = \sqrt{2Dt}$. M and D stand for measured and corrected, respectively. Note that extraction of diffusivity values was performed for the samples annealed for the longest times only, in order to ensure steady-state conditions.

3. Results

An illustration of the sample geometry prior to heat treatments, by means of ^{13}C concentration profiles as detected by SIMS, is depicted in Figure 1. The figure reveals a ^{13}C-lean epi-layer with both the C-cap and substrate acting as ^{13}C sources. Please note that the SIMS signal in the C-cap layer has not been normalized, and that no correction was performed for the lower carbon ionization yield in the pure carbon (C-cap) matrix relative to the 4H-SiC matrix. The lower ionization yield in the graphitized layer compared to 4H-SiC explains the differences in carbon concentration between the C-cap and 4H-SiC layers in Figure 1. Moreover, one should expect slightly different sputtering rates in the SIMS measurements for the C-cap and 4H-SiC material layers.

Figure 2 displays the temperature-dependent ^{13}C profiles as deduced from SIMS measurements after sequential annealing steps. The ^{13}C profiles are shown after isothermal annealing at 2300 °C for 15–230 min at the interface between the 4H-SiC substrate, which has a natural abundance of ^{13}C, and the ^{12}C isotope purified epitaxial layer in Figure 2a, at approximately 7 µm from the 4H-SiC epi-layer surface. The same interface is studied in Figure 2b, but for 15 min annealing steps in the temperature range 2300–2450 °C. Figure 2c showcases the ^{13}C profiles at the C-cap/4H-SiC interface for isochronal annealing at temperatures between 2300–2450 °C for 15 min. Indeed, Figure 2 demonstrates that C diffuses readily at both the internal 7 µm interface (4H-SiC epi-layer/substrate) and at the C-cap/4H-SiC interface above a temperature of ∼2300 °C. The profiles are fitted reliably by Equation (1), as indicated by the dotted data points and the solid fit lines in Figure 2. Due to the different ionization levels in the C-cap and 4H-SiC layers and accompanying challenges with normalization, the fitted concentration profiles for ^{13}C are only shown on the 4H-SiC epi-layer side of the interface depicted in Figure 2c. Note that the placing of the C-cap/4H-SiC interface adds some additional uncertainty to the extracted diffusivities for C moving from the C-cap layer to the isotope purified 4H-SiC material.

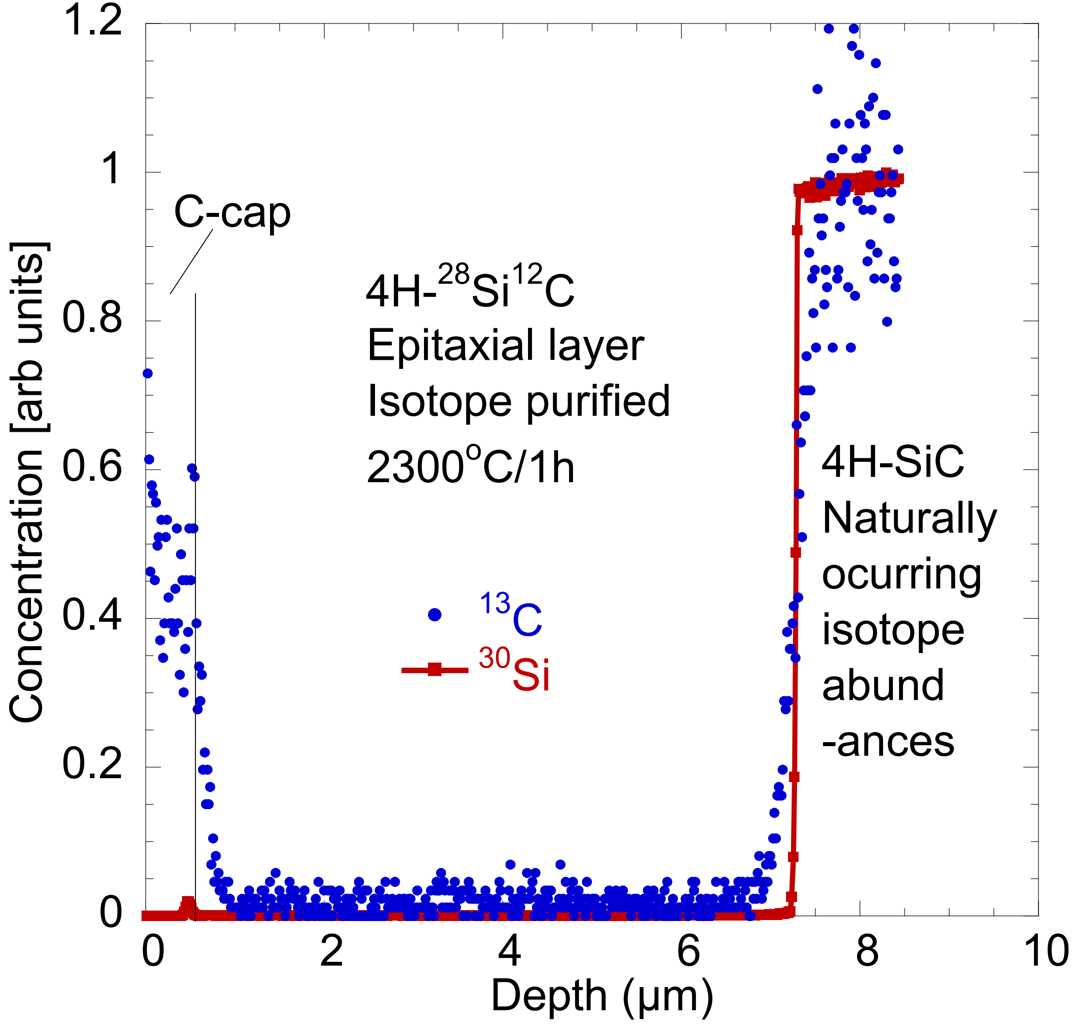

Figure 1. Overview of the sample geometry as detected by secondary ion mass spectrometry (SIMS), with ^{13}C concentration values normalized to 1 in the 4H-SiC substrate. Note that the sample was heated to 2300 °C for 1 h.

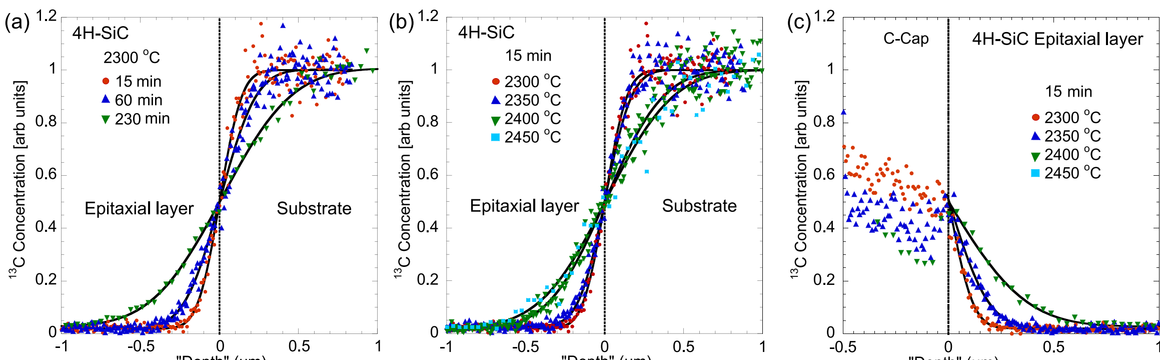

Figure 2. ^{13}C profiles as deduced by SIMS and fitted according to Equation (1), at (**a**) the interface between the isotope purified epi-layer and the substrate for 2300 °C annealing for 15–230 min, (**b**) the interface between the isotope purified epi-layer and the substrate for 2300–2450 °C annealing for 15 min, and (**c**) at the C-cap/epi-layer interface for 2300–2450 °C annealing for 15 min.

The corresponding ^{30}Si depth profiles are shown in Figure 3 at the 4H-SiC substrate/isotope purified epi-layer interface. The time dependence of Si motion at 2300 °C is highlighted in Figure 3a, and temperature dependence in Figure 3b for 15 min isochronal annealing between 2300–2450 °C.

In contrast to the ^{13}C case, the ^{30}Si profiles exhibit a small redistribution only, i.e., any self-diffusion observed for Si within the studied temperature range is significantly smaller than that found for C. Indeed, the redistribution of ^{30}Si observed for, e.g., the 2300 °C sample is similar to that measured at a reference sample (not annealed) with a C-cap (not shown in Figure 3). Note that the shoulder in the ^{30}Si profiles extending from the interface towards the surface, e.g., exhibiting a ^{30}Si concentration of 0.3 at −0.2 µm for the 230 min sample in Figure 3a, likely arises due to pinholes manifesting in the C-cap at longer annealing times and high temperatures. The pinholes were unavoidable in our SIMS experiment, but are not considered with respect to the diffusion behavior. An alternative explanation for the Si shoulder in Figure 3a related to transient diffusion is discarded, as the same profile shapes are obtained for a reference sample with a C-cap and samples annealed during 15 and 60 min. Most likely, the observed ^{30}Si profile broadening is caused by variations in the thickness and surface structure of the C-cap film. Unfortunately, for long annealing times (230 min), the C-cap starts to degrade.

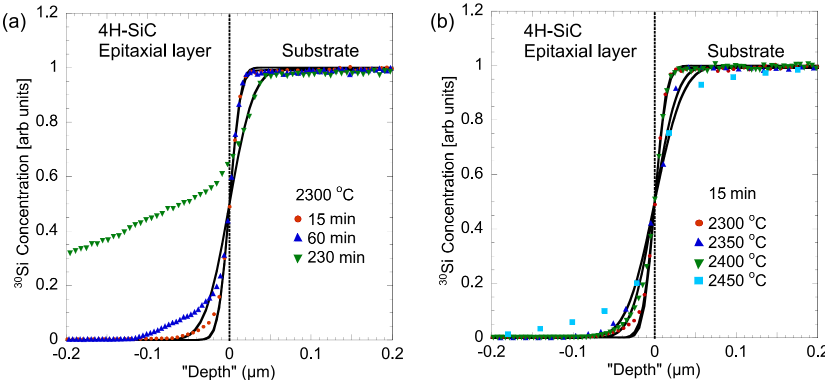

Figure 3. ^{30}Si profiles as detected by SIMS and fitted according to Equation (1), at (**a**) 2300 °C for 15, 60, and 230 min annealing, and (**b**) for annealing at various temperatures between 2300–2450 °C for 15 min. The profiles were collected at the interface between the isotope purified epi-layer and the 4H-SiC substrate, at approximately 7 µm from the epi-layer surface.

Estimated diffusivities (D) for ^{13}C (at the two interfaces) and ^{30}Si (at the internal 4H-SiC interface) are collected in Table 2. The D-values are extracted from fits to the experimental data presented in Figures 2 and 3 using Equation (1). Indeed, if one assumes that Si migration is observed in Figure 3, the Si diffusivities are at least a factor 100–1000 times lower than those for C, which agrees reasonably well with previous studies [2,5,6,28,29]. However, the high-temperature heat treatments induce surface roughening effects that complicate measurements of the Si and C depth distributions. For the 2300 °C samples, the peak-to-peak roughness is about 20 nm, which is further increasing to around 30 nm for the 2400 °C samples. From the estimated diffusivities extracted for Si from Figure 3 (see Table 2), we infer diffusion lengths for Si in the 20–30 nm range. Hence, the surface roughness is in the same range as the observed ^{30}Si diffusion lengths, meaning that the estimated ^{30}Si diffusivities must necessarily be of the same order as the uncertainty arising from the surface roughening. Therefore, the ^{30}Si D-values and redistribution depicted in Table 2 and Figure 3 must be considered as an upper bound. Moreover, due to the overlap between ^{30}Si diffusion lengths and surface roughening, the estimates for D_0 and E_A for Si self-diffusion are highly uncertain and will therefore not be quoted herein. The redistribution of ^{13}C, on the other hand, is above the surface roughness and therefore adequately represents the carbon migration. From Figures 2 and 3 combined with the above discussion, we thus infer that carbon migrates readily in 4H-SiC within a 2300–2450 °C temperature interval while silicon does not.

Table 2. Estimated diffusivities for ^{13}C and ^{30}Si migration in 4H-SiC samples under intrinsic conditions and at various temperatures. ^{13}C profiles are collected both at the interface 7 µm into the epi-layer, and at the C/4H-SiC surface, while ^{30}Si diffusivities are from the internal 4H-SiC interface only.

T (°C)	t (min)	D (cm^2/s)	D (cm^2/s)	D (cm^2/s)
		^{13}C	^{13}C	^{30}Si
		7 µm into epi	SiC/C Interface	7 µm into epi
2300	15	6.63×10^{-14}	4.45×10^{-14}	6.3×10^{-16}
2300	60	4.45×10^{-14}	3.15×10^{-14}	1.6×10^{-16}
2300	230	4.45×10^{-14}	3.02×10^{-14}	2.0×10^{-16}
2350	15	9.68×10^{-14}	8.90×10^{-14}	2.6×10^{-15}
2400	15	4.59×10^{-13}	3.94×10^{-13}	7.9×10^{-16}
2400	101	1.97×10^{-13}	1.30×10^{-13}	4.2×10^{-15}
2450	15	6.18×10^{-13}	3.80×10^{-13}	4.2×10^{-15}

Figure 4 displays the Arrhenius behavior of the carbon and silicon diffusivity values as summarized in Table 2. The diffusivities extracted for SiC samples employed both herein (No. 5 and 11, brown data points and fit) and in other works [2,5,6,28,29] are included in Figure 4, with the corresponding temperature range, migrating species, D_0, E_A value and reference collected in Table 3. Note that the data points used for the fit for No. 10 (data and fit collected from Ref. [28]) were chosen based on an upper limit for surface roughening of 15 nm.

Table 3. Collection of Arrhenius data for C and Si self-diffusion from the literature and the present work (No. 5 and 11), see also Figure 4.

No.	T Interval (°C)	Conditions	Isotope	D_0 (cm^{2}B)	E_A (eV)	Reference
1	1850–2180	Si-rich, 6H	^{14}C	8.6×10^5	7.41	[2]
2	1850–2180	Si-rich, 6H	^{14}C	3.3×10^7	8.20	[2]
3	2000–2290	Si-rich, 6H	^{30}Si	1.5×10^5	8.18	[2]
4	2000–2290	Si-rich, 6H	^{30}Si	5.0×10^2	7.22	[2]
5	2300–2450	4H	^{13}C	8.3×10^6	10.4	Present work
6	2100–2350	4H	^{13}C	8.4×10^2	8.50	[5]
7	2000–2450	4H	^{13}C	4.8×10^{-2}	6.7	[28]
8	2000–2200	4H	^{13}C and ^{30}Si	4.8	7.6	[6] Deduced in combination with B-diffusion
9	1950–2200	Probably 6H	Si	7.3×10^{-5}	5.4	[29] Deduced from B-diffusion
10	2000–2450	4H	^{30}Si	3.8×10^4	10.6	[28]
11	2300–2450	4H	^{30}Si	Uncertain	Uncertain	Present work

Importantly, our results (Table 3 and Figure 4) exhibit a significantly higher activation energy (E_A^C = 10.4 eV) and larger pre-exponential factor (D_0^C = 8.3×10^6 cm^2/s) for self-diffusion of C compared to that reported in the literature. In addition, from the extracted diffusivities collected in Table 2, we observe that the diffusivity of C decreases with time for the 2300 °C annealing, and that D is lower at the C/4H-SiC surface than at the internal interface between the CVD-grown epi-layer and the substrate at 7 µm depth. It should be noted that the data points used for representing the ^{13}C diffusivities deduced in the present work, and presented as dark brown data points (No. 5) in Figure 4, were collected at the interface located 7 µm into the 4H-SiC epi-layer (third column of Table 2), and not at the C-cap/4H-SiC surface.

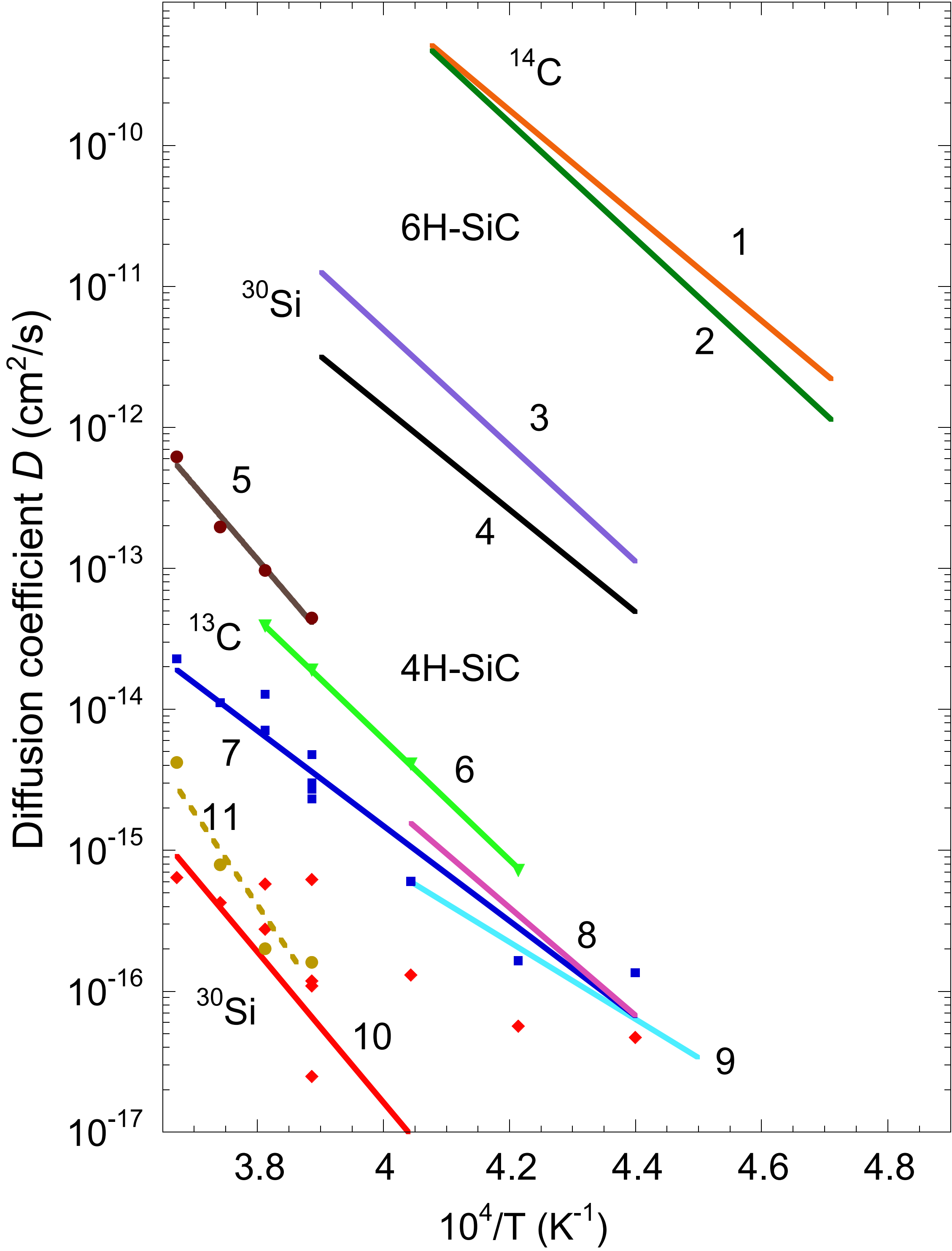

Figure 4. Arrhenius behavior of Si and C diffusivities fitted according to Equation (2), from both this work and the literature. Numbers refer to the present work (No. 5 for ^{13}C and No. 11 for ^{30}Si) and Refs. [2,5,6,28,29] (No. 1–4 and No. 6–10), with additional specifiers for the numbering collected in Table 3. Note that results in the same color are related. For example, the dark brown data points and fit refer to ^{13}C, while the light brown ones refer to ^{30}Si, both from the present work.

4. Discussion

First, let us consider the mechanisms for self-diffusion of Si and C in SiC, that is, the sub-lattice on which migration occurs and the mediating species for migration. Diffusion via antisites (Si_C and

C_{Si}) is expected to be negligible due to the high activation energies for self-diffusion via antisites, as highlighted in Table 1. Thus, we anticipate that both Si and C self-diffuse strictly on their individual sub-lattice. Importantly, self-diffusion via interstitials would first necessitate the formation of Frenkel pairs, which has not been directly calculated in any of the cited works. Self-diffusion via vacancies, on the other hand, does not have to involve Frenkel pairs, as vacancies can be injected from the surface and thereby present a means of travel for the lattice atoms. We thus conjecture that injection of vacancies from the surface, followed by Si or C atoms from the lattice propagating via the vacancies throughout the lattice, is likely associated with a lower total activation energy than Frenkel pair formation in the semiconductor bulk.

The experimental findings of the present work show a strong discrepancy when comparing to previous reports, and provide an important hint towards illuminating the process of self-diffusion in SiC. Indeed, the barrier for C self-diffusion found herein ($E_A^C = 10.4$ eV) shows agreement with neither previous experimental data (see Figure 4) nor theoretical predictions for migration via vacancies, interstitials and antisites on the C sublattice (see Table 1). Note that the high estimated pre-factor for C self-diffusion ($D_0^C = 8.3 \times 10^6$ cm^2/s) evidences that we are not, in fact, monitoring diffusion solely via fundamental nearest-neighbor atomic hops [30]. However, an intriguing difference between previous experiments and the present ones is the presence of a C-cap combined with a lower as-grown vacancy concentration, as the epitaxial growth process has improved over the years. Importantly, using a C-cap is at present a standard processing step in device fabrication, with obvious implications for the C diffusivity as carbon interstitials are injected into the material.

In Ref. [31] (on GaAs), it was proposed that self-diffusion processes with pre-factors in the 10^8–10^9 cm^2/s range indicate a self-diffusion mechanism related to Frenkel pair formation in the semiconductor bulk, which is expected to be dominant when vacancy formation is suppressed at the surface. Thus, with D_0 for C far above the 10^{-3}–10^{-2} cm^2/s expected for fundamental hops [30], it appears evident that the present findings are not representative of undisturbed self-diffusion in SiC. Instead, our results illuminate the competition between Frenkel pair formation in the bulk, and vacancy injection from the surface, as mechanisms for self-diffusion. Previous works have shown that the C-cap is responsible for continuous injection of C interstitials during high-temperature annealing [32], creating a continuous route for recombination of C vacancies that might be generated at the 4H-SiC surface under the high-temperature conditions. Moreover, the idea that C interstitials are being injected from the surface is further supported by the difference in measured C diffusivity at the surface (C-cap/4H-SiC interface) and in the bulk (isotope-pure epi-layer/substrate interface). Therefore, when there is a C-cap covering the sample surface during annealing, self-diffusion via injected vacancies is suppressed, instead pointing towards Frenkel pair formation in the bulk as the dominant route for mediating atomic redistribution. Si self-diffusion may also be impacted by the C-cap, e.g., via formation of immobile antisites.

The present experimental approach is distinctly different from that of, e.g., studying diffusion using self-implantation. For example, in Ref. [17] we tentatively attributed the mediating species for C self-diffusion in SiC to C_i. However, in samples without the C-cap, there is no permanent supply of C_i recombining with vacancy defects at the surface. Therefore, we can briefly consider both V_C and C_i as the responsible party for C self-diffusion, with E_A for self-diffusion via V_C being predicted at 9.0 eV and E_A via C_i at 7.5 eV (see Table 1). Interestingly, both values resonate well with experiment, albeit different ones; Ref. [5] predicted an E_A for ^{13}C motion of 8.5 eV, while Ref. [6] deduced that $E_A = 7.4$ eV. Indeed, the lower pre-factors for diffusion in Refs. [5,6] as compared to the present work indicate that Frenkel pair formation does not dominate in the un-capped samples, and instead we attribute C and Si self-diffusion to the formation and injection of Si and C vacancies at the surface. In fact, injection of C_i from the C-cap would delay C self-diffusion if it occurred via C vacancies, and one would expect a significant delay in C migration upon the recombination between the injected C_i and the thermally generated V_C, which would thus prevent further motion of ^{13}C atoms. A similar mechanism can be proposed for Si self-diffusion via V_{Si}, if the injected C_i form nearly immobile C_{Si}

antisites. The injection of C_i from the C-cap therefore explains both the higher activation energies and the higher pre-factors for self-diffusion deduced for C (and Si) in the present work.

5. Concluding Remarks

We investigate the effect of C injection from a carbon cap during high-temperature annealing on self-diffusion of C and Si in 4H-SiC. The continuous excess of C interstitials results in recombination of the injected C interstitials with Si and C vacancies generated in the near-surface region. Hence, the presence of the C-cap promotes the formation of Frenkel pairs in the SiC bulk as opposed to the injection of vacancies from the semiconductor surface, as evidenced by the elevated exponential pre-factors for C self-diffusion found herein as compared to previous works. In conclusion, we tentatively attribute C self-diffusion in un-capped samples to the injection of carbon vacancies from the SiC surface. The case for Si, however, is less straightforward, with predicted activation energies for Si self-diffusion overlapping regardless of whether Si vacancies or interstitials act as the mediating species. Thus, resolving Si self-diffusion on the Si sub-lattice is challenging, but following the argument for the C case, injection of Si vacancies from the surface likely outcompetes Si Frenkel pair formation when a C-cap is not present.

Author Contributions: Conceptualization, M.E.B., M.L. and L.V.; methodology, M.L., L.V., M.G. and J.U.H.; validation, M.L.; formal analysis, M.L. and M.E.B.; investigation, M.L. and L.V.; resources, M.G. and J.U.H.; writing—original draft preparation, M.E.B.; writing—review and editing, M.E.B., M.L., L.V. and J.U.H.; visualization, M.E.B. and M.L. All authors have read and agreed to the published version of the manuscript.

Funding: Financial support was kindly provided by the Research Council of Norway and the University of Oslo through the frontier research project FUNDAMeNT (no. 251131, FriPro ToppForsk-program). The Research Council of Norway is acknowledged for the support to the Norwegian Micro- and Nano-Fabrication Facility, NorFab, project number 245963. J.U.H. would like to acknowledge support from the Swedish Energy Agency Energimyndigheten project number 43611-1.

Acknowledgments: The authors would like to thank the late B.G. Svensson for contributing to the idea for this study.

Conflicts of Interest: The authors declare no conflicts of interest.

References

1. Hon, M.H.; Davis, R.F. Self-diffusion of ^{14}C in polycrystalline β-SiC. *J. Mater. Sci.* **1979**, *14*, 2411, ISSN 1573-4803. [CrossRef]
2. Hong, J.D.; Hon, M.H.; Davis, R.F. Self-diffusion in alpha and beta silicon carbide. *Ceramurg. Int.* **1979**, *5*, 155. [CrossRef]
3. Hon, M.H.; Davis, R.F.; Newbury, D.E. Self-diffusion of ^{30}Si in polycrystalline β-SiC. *J. Mater. Sci.* **1980**, *15*, 2073, ISSN 1573-4803. [CrossRef]
4. Hong, J.D.; Davis, R.F. Self-Diffusion of Carbon-14 in High-Purity and N-Doped α-SiC Single Crystals. *J. Am. Ceram. Soc.* **1980**, 63, 546. [CrossRef]
5. Linnarsson, M.K.; Janson, M.S.; Zhang, J.; Janzén, E.; Svensson, B.G. Self-diffusion of ^{12}C and ^{13}C in intrinsic 4H–SiC. *J. Appl. Phys.* **2004**, *95*, 8469. [CrossRef]
6. Rüschenschmidt, K.; Bracht, H.; Stolwijk, N.A.; Laube, M.; Pensl, G.; Brandes, G.R. Self-diffusion in isotopically enriched silicon carbide and its correlation with dopant diffusion. *J. Appl. Phys.* **2004**, *96*, 1458. [CrossRef]
7. Bockstedte, M.; Mattausch, A.; Pankratov, O. Ab initio study of the migration of intrinsic defects in 3C-SiC. *Phys. Rev. B* **2003**, *68*, 205201. [CrossRef]
8. Bedoya-Martínez, O.N.; Roma, G. Activation entropies for diffusion in cubic silicon carbide from first principles. *Phys. Rev. B* **2010**, *82*, 134115. [CrossRef]
9. Negoro, Y.; Katsumoto, K.; Kimoto, T.; Matsunami, H. Electronic behaviors of high-dose phosphorus-ion implanted 4H–SiC (0001). *J. Appl. Phys.* **2004**, *96*, 224. [CrossRef]

10. Sundaresan, S.G.; Mahadik, N.A.; Qadri, S.B.; Schreifels, J.A.; Tian, Y.-L.; Zhang, Q.; Gomar-Nadal, E.; Rao, M.V. Ultra-low resistivity Al^{+} implanted 4H–SiC obtained by microwave annealing and a protective graphite cap. *Solid-State Electron.* **2008**, *52*, 140. [CrossRef]
11. Nipoti, R.; Mancarella, F.; Moscatelli, F.; Rizzoli, R.; Zampolli, S.; Ferri, M. Carbon-Cap for Ohmic Contacts on Ion-Implanted 4H-SiC. *Electrochem. Solid-State Lett.* **2010**, *13*, H432. [CrossRef]
12. Kobayashi, T.; Harada, K.; Kumagai, Y.; Oba, F.; Matsushita, Y. Native point defects and carbon clusters in 4H-SiC: A hybrid functional study. *J. Appl. Phys.* **2019**, *125*,125701. [CrossRef]
13. Coutinho, J.; Torres, V.J.B.; Demmouche, K.; Öberg, S. Theory of the carbon vacancy in 4H-SiC: Crystal field and pseudo-Jahn-Teller effects. *Phys. Rev. B* **2017**, *96*, 174105. [CrossRef]
14. Bathen, M.E.; Galeckas, A.; Müting, J.; Ayedh, H.M.; Grossner, U.; Coutinho, J.; Frodason, Y.K.; Vines, L. Electrical charge state identification and control for the silicon vacancy in 4H-SiC. *NPJ Quantum Inf.* **2019**, *5*, 111. [CrossRef]
15. Klein, P.B.; Shanabrook, B.V.; Huh, S.W.; Polyakov, A.Y.; Skowronski, M.; Sumakeris, J.J.; O'Loughlin, M.J. Lifetime-limiting defects in n- 4H-SiC epilayers. *Appl. Phys. Lett.* **2006**, *88*, 052110. [CrossRef]
16. Weber, J.R.; Koehl, W.F.; Varley, J.B.; Janotti, A.; Buckley, B.B.; Van de Walle, C.G.; Awschalom, D.D. Quantum computing with defects. *Proc. Natl. Acad. Sci. USA* **2010**, *107*, 8513. [CrossRef]
17. Bathen, M.E.; Coutinho, J.; Ayedh, H.M.; Ul Hassan, J.; Farkas, I.; Öberg, S.; Frodason, Y.K.; Svensson, B.G.; Vines, L. Anisotropic and plane-selective migration of the carbon vacancy in SiC: Theory and experiment. *Phys. Rev. B* **2019**, *100*, 014103. [CrossRef]
18. Heyd, J.; Scuseria, G.E.; Ernzerhof, M. Hybrid functionals based on a screened Coulomb potential. *J. Chem. Phys.* **2003**, *118*, 8207. [CrossRef]
19. Mills, G.; Jónsson, H. Quantum and thermal effects in H_2 dissociative adsorption: Evaluation of free energy barriers in multidimensional quantum systems. *Phys. Rev. Lett.* **1994**, *72*, 1124. [CrossRef]
20. Mills, G.; Jónsson, H.; Schenter, G.K. Reversible work transition state theory: application to dissociative adsorption of hydrogen. *Surf. Sci.* **1995**, *324*, 305. [CrossRef]
21. Henkelman, G.; Jónsson, H. A dimer method for finding saddle points on high dimensional potential surfaces using only first derivatives. *J. Chem. Phys.* **1999**, *111*, 7010. [CrossRef]
22. Kuate Defo, R.; Zhang, X.; Bracher, D.; Kim, G.; Hu, E.; Kaxiras, E. Energetics and kinetics of vacancy defects in 4H-SiC. *Phys. Rev. B* **2018**, *98*, 104103. [CrossRef]
23. Perdew, J.P.; Burke, K.; Ernzerhof, M. Generalized Gradient Approximation Made Simple. *Phys. Rev. Lett.* **1996**, *77*, 3865. [CrossRef] [PubMed]
24. Yan, X.; Li, P.; Kang, L.; We, S.-H.; Huang, B. First-principles study of electronic and diffusion properties of intrinsic defects in 4H-SiC. *J. Appl. Phys.* **2020**, *127*, 085702. [CrossRef]
25. Son, N.T.; Trinh, X.T.; Løvlie, L.S.; Svensson, B.G.; Kawahara, K.; Suda, J.; Kimoto, T.; Umeda, T.; Isoya, J.; Makino, T.; et al. Negative-*U* System of Carbon Vacancy in 4H-SiC. *Phys. Rev. Lett.* **2012**, *109*, 187603. [CrossRef] [PubMed]
26. Wang, X.; Zhao, M.; Bu, H.; Zhang, H.; He, X.; Wang, A. Formation and annealing behaviors of qubit centers in 4H-SiC from first principles. *J. Appl. Phys.* **2013**, *114*, 194305. [CrossRef]
27. Iwamoto, N.; Svensson, B.G. Chapter Ten—Point Defects in Silicon Carbide. In *Defects in Semiconductors*; Romano, L., Privitera, V., Jagadish, C., Eds.; Volume 91 of Semiconductors and Semimetals; Elsevier: Amsterdam, The Netherlands, 2015; pp. 369–407.
28. Rüschenschmidt, K. Selbst- und Fremddiffusion in Siliziumkarbid zur Charakterisierung der atomaren Eigenpunktdefekte. Ph.D. Thesis, Westfälischen Wilhelms-Universität Münster, Münster, Germany, 2006.
29. Konstantinov, A.O. Nature of point defects generated during diffusion of acceptor impurities in silicon carbide. *Sov. Phys. Semicond.* **1992**, 26, 151.
30. Philibert, J. *Atom Movements: Diffusion and Mass Transport in Solids*; Editions de Physique: Les Ulis, France, 1991; ISBN 9782868831613.

31. Wager, J.F. Energetics of self-diffusion in GaAs. *J. App. Phys.* **1991**, *69*, 3022. [CrossRef]
32. Ayedh, H.M.; Nipoti, R.; Hallén, A.; Svensson, B.G. Elimination of carbon vacancies in 4H-SiC employing thermodynamic equilibrium conditions at moderate temperatures. *Appl. Phys. Lett.* **2015**, *107*, 252102. [CrossRef]

© 2020 by the authors. Licensee MDPI, Basel, Switzerland. This article is an open access article distributed under the terms and conditions of the Creative Commons Attribution (CC BY) license (http://creativecommons.org/licenses/by/4.0/).